Frontiers in Bioscience Landmark

Front. Biosci. (Landmark Ed) **2026**; 31(6): 50519
https://doi.org/10.31083/FBL50519

Original Research

TRIM68 Exacerbates Sepsis-induced Liver Injury by Inhibiting TIP60-dependent autophagy

Yousong Xu[1,2], Xueping Yang[2], Xiaoming Chen[2], Huifeng Yuan[2,*], Min Shao[1,*]

[1]Department of Critical Care Medicine, The First Affiliated Hospital of Anhui Medical University, 230022 Hefei, Anhui, China
[2]Department of Critical Care Medicine, The Third Affiliated Hospital of Anhui Medical University, 230061 Hefei, Anhui, China
*Correspondence: yhf68301@163.com (Huifeng Yuan); shaomin@ahmu.edu.cn (Min Shao)
Academic Editor: Graham Pawelec
Submitted: 29 January 2026 Revised: 28 April 2026 Accepted: 20 May 2026 Published: 24 June 2026

Abstract

Background: Sepsis-induced liver injury (SILI) is a major contributor to mortality in critically ill patients, yet the temporal regulation and functional significance of autophagy in SILI remain poorly defined. Defining the dynamic changes in autophagy and the underlying molecular mechanisms is therefore essential for the development of effective therapies. **Methods**: We integrated public transcriptomic datasets from human and murine SILI with *in vivo* and *in vitro* experimental models to characterize the dynamic regulation of autophagy and identify key regulatory factors. Genetic gain- and loss-of-function approaches targeting tripartite motif containing 68 (TRIM68) were combined with cecal ligation and puncture (CLP) mouse models and LPS-stimulated hepatocytes. These methods were coupled with molecular, biochemical, and imaging analyses, including quantitative reverse transcription polymerase chain reaction (qRT–PCR), western blotting, immunofluorescence, transmission electron microscopy, enzyme-linked immunosorbent assay (ELISA), cleavage under targets and tagmentation (CUT-Tag), coimmunoprecipitation, and ubiquitination assays, to elucidate the underlying mechanisms. **Results**: Autophagy was dynamically regulated during SILI, with early activation followed by a decrease that coincided with aggravated liver injury and inflammation. Enhancing autophagy significantly alleviated hepatic injury and inflammatory responses. Integrative analyses identified TRIM68 as a conserved autophagy-associated regulator across human and murine SILI. Loss of TRIM68 expression enhanced autophagic flux and reduced proinflammatory cytokine production. Mechanistically, TRIM68 loss stabilized TIP60 by reducing its ubiquitination and proteasomal degradation, thereby enhancing the histone H4 acetylation–dependent transcription of autophagy-related genes. **Conclusion**: Our findings identify TRIM68 as a key epigenetic regulator of autophagy in sepsis-induced liver injury, mediating TIP60-dependent histone H4 acetylation to drive autophagy gene transcription, and support the therapeutic potential of targeting the TRIM68–TIP60 axis.

Keywords: sepsis; autophagy; liver failure; tripartite motif proteins; lysine acetyltransferase 5

1. Introduction

Sepsis is a life-threatening syndrome characterized by dysregulated host immune responses and remains a leading cause of mortality in intensive care units worldwide [1]. Excessive inflammatory activation and cytokine storms frequently lead to widespread cellular injury and multiple organ dysfunction [1,2,3]. The liver, as a central organ in metabolic and immune regulation, is particularly susceptible to septic insult, and sepsis-induced liver injury (SILI) is closely associated with disease severity and mortality [4,5]. However, the mechanisms underlying acute hepatic dysfunction in sepsis remain incompletely understood, and effective targeted therapies are lacking.

Autophagy is a conserved intracellular degradation process that is essential for maintaining hepatocellular homeostasis through the clearance of damaged organelles and misfolded proteins [6,7]. In SILI, autophagy serves as a crucial protective mechanism that limits hepatocyte damage under inflammatory and metabolic stress [6,7,8]. Evidence from hepatocyte-specific Atg5 or Atg7 knockout mouse models has demonstrated that disruption of autophagic flux markedly exacerbates liver injury and increases mortality during sepsis, highlighting the importance of intact autophagy in maintaining hepatic resilience [9,10]. Clinical observations further support this concept: liver specimens from septic patients exhibit abundant autophagic vacuoles, and the accumulation of autophagosomes is accompanied by impaired autophagosome–lysosome fusion in the livers of septic patients [11]. Pharmacological restoration of autophagic flux, including agents such as carbamazepine, dexmedetomidine, and genipin, alleviates septic liver injury in preclinical models, underscoring the therapeutic relevance of functional autophagy [12,13]. Despite these insights, the molecular regulators governing autophagy dynamics during sepsis remain incompletely understood, and identifying novel upstream modulators is essential for advancing therapeutic strategies for SILI.

Here, through integrated transcriptomic analyses of human and murine SILI combined with *in vivo* and *in vitro* validation, we identify tripartite motif containing 68 (TRIM68) as a previously unrecognized negative regulator of autophagy. We show that TRIM68 suppresses au-

tophagy by promoting TIP60 ubiquitination and degradation, thereby reducing histone H4 acetylation-dependent transcription of autophagy-related genes. These findings establish TRIM68 as a key epigenetic regulator of autophagy and highlight the TRIM68–TIP60 axis as a potential therapeutic target in sepsis-induced liver injury.

2. Methods

2.1 Data Acquisition

We retrieved three sepsis-induced liver injury datasets from the GEO database: one transcriptomic dataset from liver tissues from mice with sepsis-induced liver injury (GSE167277) and two from peripheral blood samples from patients with sepsis-related liver injury (GSE142255 and GSE156382). Specifically, the GSE167277 dataset includes liver tissue transcriptomes from mice treated with intraperitoneal LPS for 24 hours, along with a control group of wild-type mice receiving intraperitoneal saline. The GSE142255 dataset contains 7 control samples and 8 patients with acute-on-chronic liver failure induced by sepsis. GSE156382 includes 5 control samples and 6 samples from patients with sepsis-induced liver failure, as well as additional ACLF cases caused by other factors.

2.2 Differentially Expressed Autophagy-related Genes

Batch effects across different datasets were corrected using the R packages "limma" and "sva". Differentially expressed genes (DEGs) between patients with sepsis-induced liver injury and normal samples were identified with the "limma" package in R, using a cutoff of adj.p. Val < 0.05 and |logFC| >0.5. For murine data, DEGs were defined using DESeq2 with adjusted $p < 0.05$ and $|\log_2 FC| > 1$. To further identify autophagy-related DEGs, we intersected the DEGs with a curated set of autophagy-related genes. Volcano plots were generated using the "ggplot2" package, and a Venn diagram was created using an online tool (https://bioinformatics.psb.ugent.be/webtools/Venn/).

Autophagy-related genes were sourced from several databases, including REACTOME (REACTOME_AUTOPHAGY), WP (WP_AUTOPHAGY), KEGG (KEGG_REGULATION_OF_AUTOPHAGY), and GO (GOBP_REGULATION_OF_AUTOPHAGY). After duplicates were merged and removed, a total of 485 autophagy-related genes were compiled into the final dataset.

2.3 Pathway and Functional Enrichment Analysis

Pathway and functional enrichment analyses were performed using the "clusterProfiler" package. Volcano plots and box plots for differentially expressed genes were generated with the "ggplot2" package, and heatmaps were generated using the "pheatmap" package.

2.4 Mouse Experiments

Male C57BL/6J mice were purchased from Charles River Laboratories (Beijing, China) or HuaChuang Sino (Jiangsu, China) and housed in a pathogen-free environment with a 12-hour light/dark cycle and ad libitum access to food and water. All animal experiments were approved by the Animal Ethics Committee of Anhui Medical University (LLSC20242499).

A sepsis model was established using the cecal ligation and puncture (CLP) method [14]. Mice were anesthetized with 3–5% isoflurane (R510-22-10, RWD Life Science Co., Ltd., Shenzhen, Guangdong, China) in an induction chamber for 2–3 minutes, followed by maintenance at 1–3% isoflurane with a mask, monitored by breathing rate and absence of toe pinch reflex. The abdomen was sterilized using 75% alcohol, after which a 2 cm incision along the midline was made to reveal the cecum. A sterile 4-0 silk suture was used to ligate the cecum at its distal end, and a sterile needle was used for the puncture. A small amount of intestinal contents was expressed to confirm patency. The cecum was repositioned, and the incision was closed. For fluid resuscitation, 0.9% sodium chloride solution (37 °C) was subcutaneously injected at 5 mL/kg body weight. Mice were returned to a temperature-controlled room (22 °C) and monitored every 6 hours post-surgery. In the control (sham) group, the mice underwent the same procedure without ligation or puncture. Sample sizes were determined based on previous published studies using similar experimental models and our prior experience with animal experiments. All mice were randomly assigned to the experimental groups using a random number table.

For tissue collection, mice were euthanized in a sealed chamber with CO_2 gradually introduced at 30% chamber volume per minute, resulting in rapid loss of consciousness within 2–3 minutes. Respiratory status and eye color were monitored to confirm unconsciousness. Once respiration ceased, CO_2 was administered for an additional minute to ensure death, followed by immediate tissue collection. Mice that died because of surgical complications or severe CLP-induced injury before the planned tissue collection time point were excluded from subsequent liver tissue analyses.

2.5 High-Pressure Hydrodynamic Tail Vein Injection for TRIM68 Knockdown Plasmids

Six- to eight-week-old male C57BL/6J mice were used. TRIM68 knockdown plasmid (20 μg/mouse) or control plasmid, along with SB13 transposase plasmid (10 μg/mouse), was mixed with a total of 30 μg of DNA per mouse in sterile saline. Mice were prewarmed at 37 °C for 5 minutes to aid in tail vein expansion. Under anesthesia, the tail was disinfected, and a 27G or 28G needle was inserted. The plasmid solution (2 mL) was injected rapidly within 5–8 seconds, confirming correct needle placement by smooth movement within the vein. After injection, pressure was

applied for 30–60 seconds to prevent bleeding. Mice were monitored for 30 minutes for adverse reactions and used for the subsequent CLP model 2 weeks later.

2.6 Liver Function Analysis

Blood was collected from the inferior vena cava, incubated at 4 °C for clotting, and centrifuged (3000 rpm, 10 min) to obtain serum. Liver function was assessed by measuring serum ALT and AST levels using an automated biochemical analyzer.

2.7 Histology and H&E Staining

Liver tissue samples were harvested, fixed in 4% paraformaldehyde (BL539A, Biosharp, Guangzhou Saiguo Biotech Co., LTD, Guangzhou, Guangdong, China) at 4 °C for 24 hours, and then processed for paraffin embedding. Slides were prepared by cutting sections with a thickness of 4 µm, which were then mounted on glass and stained using hematoxylin and eosin (H&E) following standard protocols. After staining, the slides were dehydrated, cleared, and coverslipped. Histopathological changes were assessed in a blinded manner, and images were captured using an Olympus VS200 microscope equipped with a digital camera (Olympus Corporation, Tokyo, Japan).

2.8 TUNEL Fluorescence Staining

Apoptotic cells in tissue sections were detected using a terminal deoxynucleotidyl transferase-mediated dUTP nick-end labeling (TUNEL) assay with a CF488 TUNEL Cell Apoptosis Detection Kit (G1504-100T, Servicebio, Wuhan, China) according to the manufacturer's instructions. Fluorescence imaging was conducted with a fluorescence microscope, and apoptotic cells were quantified using ImageJ software (Version 1.53, National Institutes of Health, Bethesda, MD, USA).

2.9 Multiplex Immunofluorescence Staining of Liver Tissue Sections

Liver tissue sections (4–5 µm) from FFPE samples were deparaffinized, rehydrated through ethanol gradients, and subjected to antigen retrieval in sodium citrate (pH 6.0) or EDTA (pH 9.0) buffer by microwaving for 20 minutes. After they cooled, the sections were treated with 3% hydrogen peroxide (H_2O_2) for 20 minutes to block endogenous peroxidase activity. Following incubation with 5% bovine serum albumin (BSA) for 1 hour at room temperature, primary antibodies were applied overnight at 4 °C. After being washed, the sections were incubated with secondary antibodies (100 µL, PV-6000, Zsbio, Beijing, China) for 1 hour at room temperature. Signal amplification was performed using TSA fluorescence reagent for 1–3 minutes. This process was repeated for each target antibody. After the final antibody incubation, the sections were stained with DAPI. Imaging was performed with a confocal microscope, and protein expression and colocalization were analyzed based on fluorescence signals. Primary antibodies against LC3B (1:500, 81004-1-RR, Proteintech, Wuhan, China), HNF4α (1:200, ab201460, Abcam, Cambridge, UK), TIP60 (1:200, 12058, Cell Signaling Technology, Danvers, Massachusetts, USA) and TRIM68 (1:200, PA5-99785, Thermo Fisher Scientific, Massachusetts, USA) were used.

2.10 Transmission Electron Microscopy (TEM)

After the mice were euthanized, liver tissues were fixed in 2.5% glutaraldehyde (pH 7.4) at 4 °C for 4 hours, then washed in PBS and postfixed in 1% osmium tetroxide for 2 hours. The tissues were dehydrated in ethanol (30%, 50%, 70%, 90%, and 100%) and infiltrated with acetone, followed by embedding in epoxy resin. Ultrathin sections (60–80 nm) were cut using a microtome (Leica EM UC7, Leica Camera AG, Wetzlar, Germany), stained with uranyl acetate and lead citrate, and examined with a transmission electron microscope (Tecnai T12 Biotwin, FEI Company, Hillsboro, USA). The ultrastructures of hepatocytes, including autophagosomes and mitochondria, were observed at appropriate magnifications.

2.11 Quantitative Reverse Transcription (qRT) PCR

Total RNA was isolated from samples using TRIzol reagent (15596026, Thermo Fisher, Massachusetts, USA). Reverse transcription was carried out using SuperMix following the manufacturer's protocol (11151ES60, Yeasen, Shanghai, China). PCR amplification was performed using SYBR Master Mix (Yeasen, 11185ES08), and relative mRNA levels were quantified using the $\Delta\Delta$CT method and normalized to those of GAPDH. The primer sequences are listed in **Supplementary Table 1**.

2.12 Western Blot

Tissues were homogenized in RIPA buffer supplemented with protease and phosphatase inhibitors. For cells, lysis buffer was applied, followed by scraping. The homogenates were subsequently centrifuged at 12,000 rpm for 20 minutes at 4 °C, after which the supernatants were collected. The protein concentration was determined by a BCA assay. Equal amounts of protein were mixed with 2× SDS–PAGE sample buffer and heated at 95 °C for 5 minutes. After 40 µg of protein samples were separated by SDS–PAGE, the proteins were transferred onto PVDF membranes, which were subsequently blocked with 5% skim milk for 1 hour. The membranes were incubated with primary antibodies overnight at 4 °C, washed, and incubated with secondary antibodies (1:4000, SA00001-1/SA00001-2, Proteintech, Wuhan, China) for 1 hour. The signals were detected using ECL reagent (61089/31060, SUDGEN, Nanjing, Jiangsu, China) and a Tanon 5200 system (Tanon, Shanghai, China). Primary antibodies against BECLIN1 (1:1000, 11306-1-AP, Proteintech, Wuhan, China), LC3B (1:1000, ab192890, Abcam, Cambridge, UK), p62/SQSTM1(1:1000, 18420-1-AP, Pro-

teintech, Wuhan, China) and GAPDH (1:3000, 60004-1-Ig, Proteintech, Wuhan, China) were used.

2.13 Cell Lines

HepG2 cells were obtained from Wuhan Procell Life Technology Co., Ltd. (Wuhan, China), and HEK293T cells (SCSP-502) were obtained from the Shanghai Institute of Cell Biology, Chinese Academy of Sciences (China). Both cell lines were cultured in DMEM (GIBCO, C11995500BT) supplemented with 10% FBS (BI, 10270–106) in a 37 °C, 5% CO_2 humidified incubator. All the cell lines were validated by STR profiling and tested negative for mycoplasma. HepG2 and HEK293T cells between passages 3 and 15 were used for all experiments.

2.14 Immunofluorescence Staining

Cultured cells were washed twice with room temperature TBS, followed by fixation with 4% paraformaldehyde in TBS at 4 °C for 15 minutes. After fixation, the cells were rinsed three times with cold TBS for 5 minutes each. The samples were blocked with 5% goat serum at 37 °C for 30 minutes. After blocking, primary antibodies were added and incubated overnight at 4 °C. The next day, the cells were washed with TBST and TBS buffers, followed by incubation with secondary antibodies at room temperature for 1 hour in the dark. After further washing, DAPI was applied to stain the nuclei for 10 minutes. Finally, the cells were mounted with an anti-fade reagent and visualized using a fluorescence microscope. Primary antibodies against LC3B (1:200, ab192890, Abcam, Cambridge, UK), TIP60 (1:200, 12058, Cell Signaling Technology, Danvers, Massachusetts, USA) and TRIM68 (1:200, PA5-99785, Thermo Fisher Scientific, Massachusetts, USA) were used.

2.15 Plasmids

Stable knockdown cell lines were generated by transfecting HEK293T cells with lentiviral packaging plasmids (psPAX2 and pMD2.G) and shRNA constructs (**Supplementary Table 2**) at a 2:2:1 ratio. After 48 hours, the viral supernatants were collected, filtered through 0.45 µm filters, and used to infect target cells in the presence of 8 µg/mL polybrene. Infected cells were selected with puromycin. For transient overexpression, plasmid transfection was performed using Lipofectamine 3000 (Invitrogen) following established procedures.

2.16 Cell Death Assay

Cells were seeded in 12-well plates overnight in complete medium and then treated with LPS and autophagy inhibitors as specified. After staining with PI and Hoechst, cell death was quantified as the ratio of PI-positive to Hoechst-stained cells.

2.17 CUT&Tag Assays and Analysis

CUT&Tag assays were performed in accordance with the manufacturer's instructions (Novoprotein, N259-YH01). In brief, 1×10^5 cells were immobilized on Concanavalin A-coated magnetic beads for 15 minutes and permeabilized with 0.05% digitonin. After overnight incubation with primary antibody (Anti-acetyl-Histone H4 Antibody, Merck, 06866) at 4 °C, the cells were incubated with a secondary antibody conjugated to protein A/G. Tagmentation was performed using pA–Tn5 transposase at 37 °C for 1 hour and then terminated with 10% SDS and proteinase K at 55 °C for 10 minutes. Libraries were amplified by PCR (12–18 cycles), purified, and size-selected. The sequencing process was conducted using the Illumina NovaSeq 6000 platform, generating ≥20 million uniquely mapped reads per sample.

Raw data were processed with fastp (version 0.44, https://github.com/OpenGene/fastp), including adapter trimming, sliding window quality filtering (Q15), and a minimum read length of 30 bp. Clean reads were aligned to the human reference genome (hg38) using Bowtie2 (version 2.5, https://github.com/BenLangmead/bowtie2) with the --very-sensitive preset. SAMtools (version 1.19, https://github.com/samtools/samtools) was used to filter and sort the BAM files, and duplicates were removed with sambamba (version 0.8, https://github.com/biod/sambamba). Mitochondrial reads were excluded. CPM-normalized bigWig files were generated using deepTools (version 3.5, Max Planck Institute for Immunobiology and Epigenetics, Freiburg, Germany) and visualized in IGV (version 2.16, https://igv.org/).

2.18 Coimmunoprecipitation (Co-IP) Assay

Cells were transfected with FLAG-tagged TRIM68 (FLAG-TRIM68) and either HA-tagged TIP60 (HA-TIP60) or the HA empty vector (HA-NC) using a commercial transfection reagent. After 24–48 hours, the cells were washed with ice-cold PBS and lysed in IP buffer (50 mM Tris-HCl, pH 7.4; 150 mM NaCl; 1% NP-40; 1 mM EDTA) containing protease inhibitors. The lysates were incubated on ice for 30 minutes and clarified by centrifugation at 12,000 ×g for 15 minutes at 4 °C. One-third of the supernatant was kept as input, and the remainder was incubated with anti-FLAG agarose beads for preclearing, followed by overnight incubation with anti-FLAG antibody.

Immune complexes were captured using FLAG agarose beads for 1–2 hours, washed 4–5 times with lysis buffer, and eluted by boiling in 2 × SDS loading buffer. Proteins were analyzed by SDS–PAGE and immunoblotting. Coimmunoprecipitated TIP60 was detected with an anti-HA antibody, and input lysates were used as loading controls.

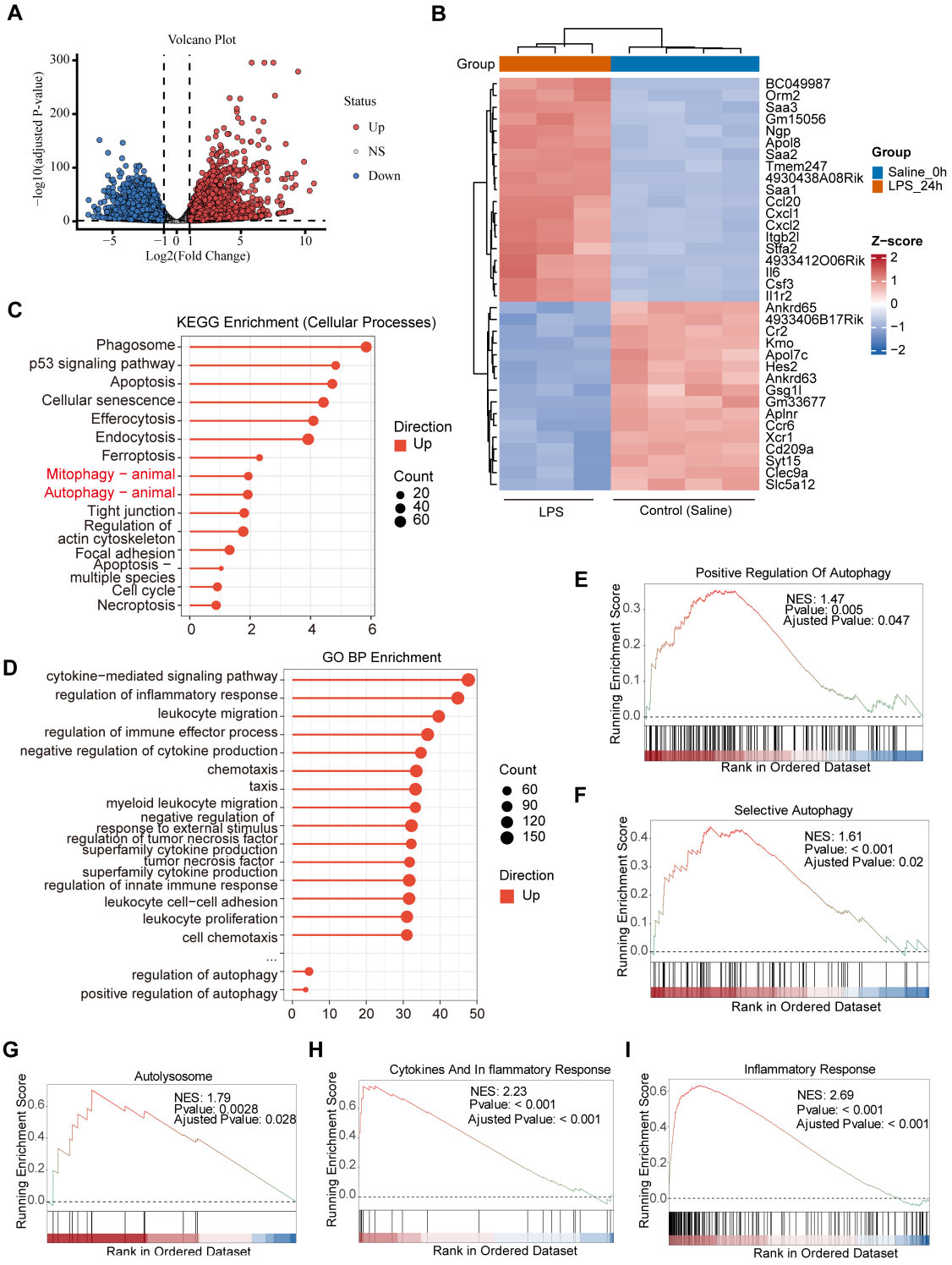

Fig. 1. Activation of autophagy and the inflammatory response in sepsis-induced liver injury. (A,B) Volcano plot (A) and heatmap (B) showing genes that were differentially expressed between the LPS-treated and saline-treated groups at 24 hours based on the GSE167277 dataset from the GEO database. (C,D) KEGG enrichment of upregulated genes in the "cellular processes" category (C) and GO biological process (BP) enrichment results (D). (E–I) GSEA results showing positive enrichment of pathways related to autophagy (E–G) and the inflammatory response (H,I).

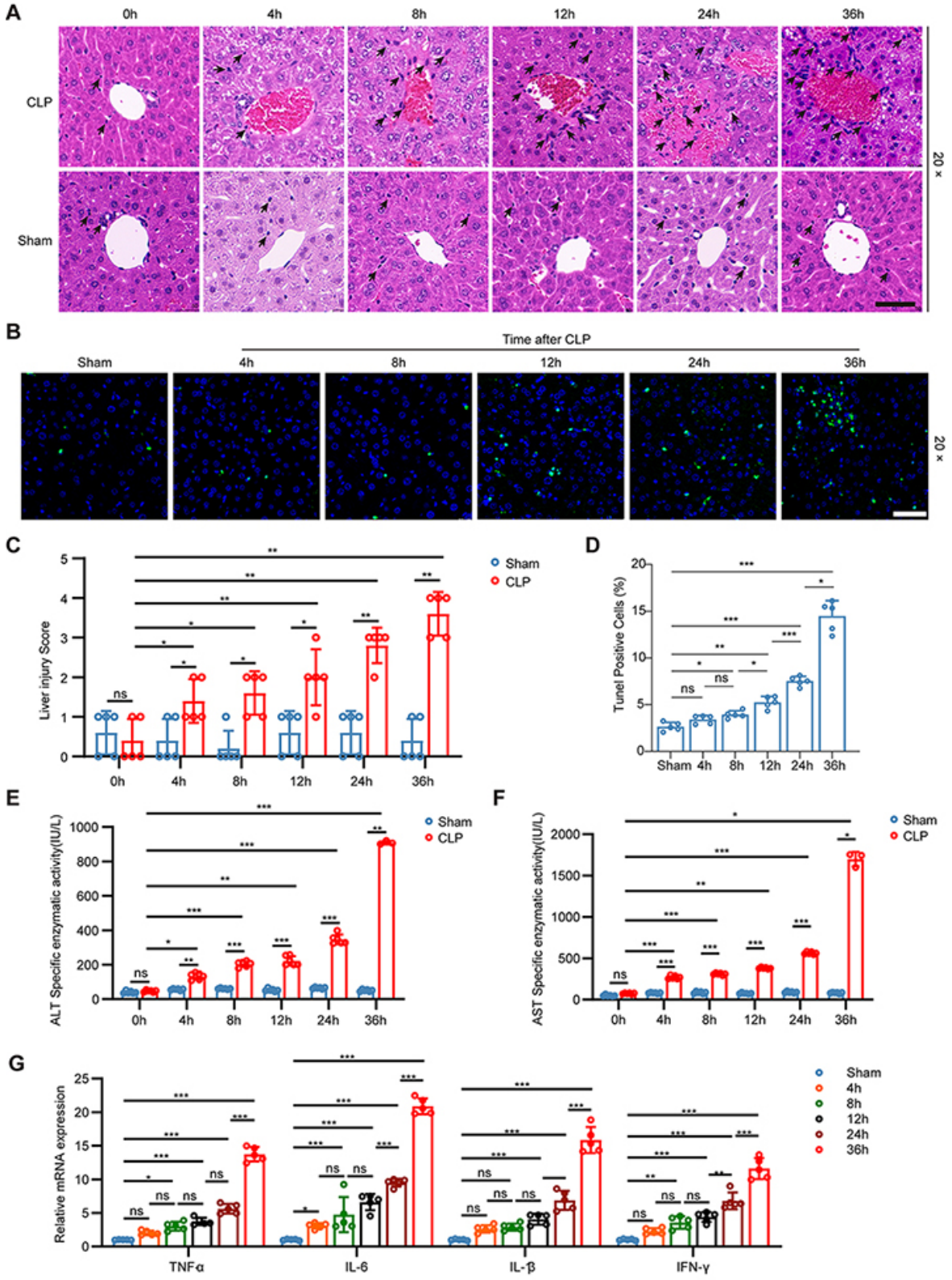

Fig. 2. Progressive liver injury and inflammation in CLP-induced sepsis. (A,B) Representative H&E-stained liver sections (A) and TUNEL staining (B) from sham and CLP mice at the indicated time points. Scale bar: 50 μm. (C,D) Quantification of liver injury scores (C) and TUNEL-positive cells (D) (n = 5 per group). (E,F) Serum ALT (E) and AST (F) levels at the indicated time points post-CLP. (G) mRNA levels of inflammation-related genes in liver tissue from sham and CLP mice. (C–G) Data are presented as the mean ± SD; *$p < 0.05$; **$p < 0.01$; ***$p < 0.001$; ns = not significant; one-way ANOVA (D), two-way ANOVA (C,E–G).

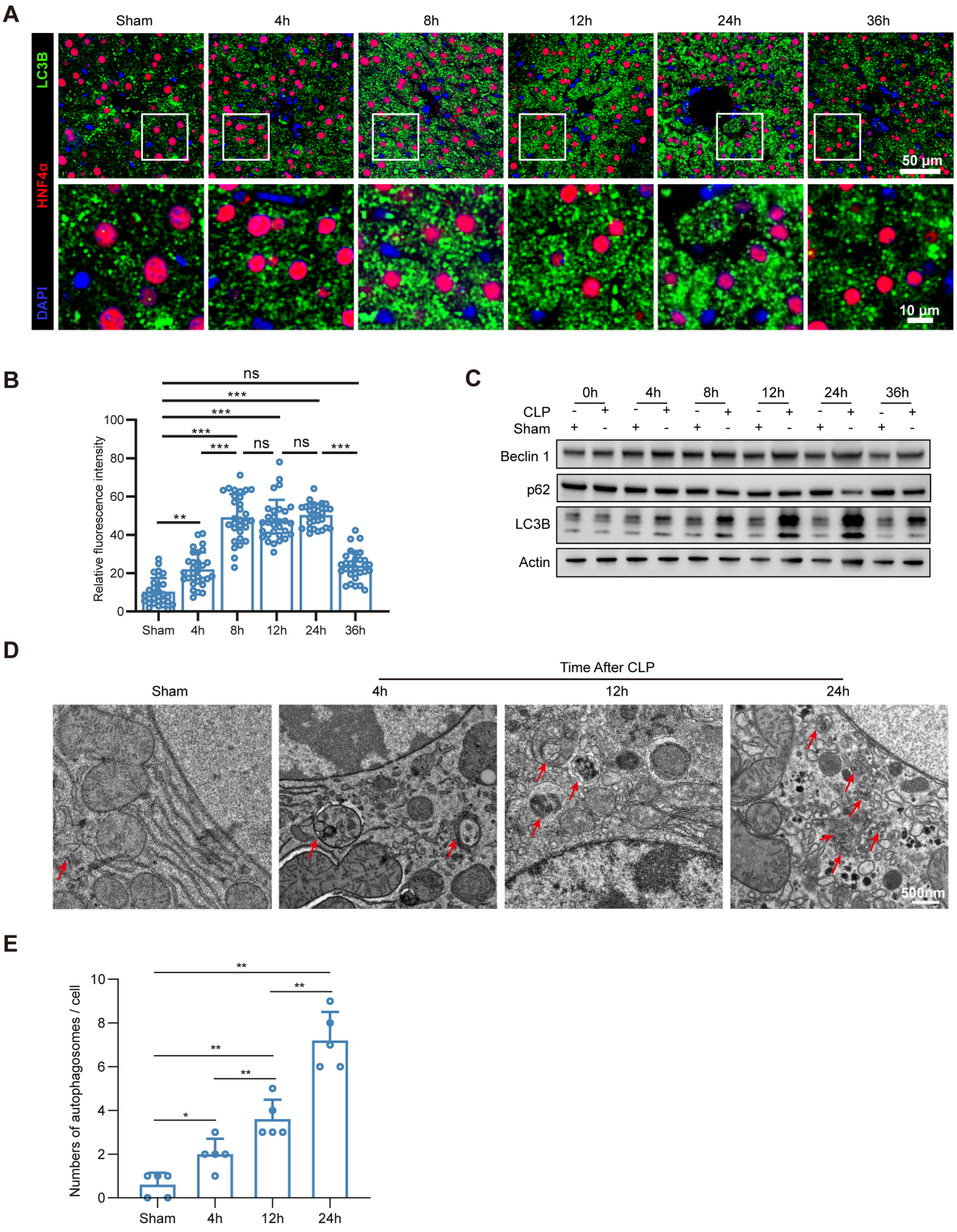

Fig. 3. Temporal dynamics of autophagy in sepsis-induced liver injury. (A) LC3B immunofluorescence in sham and CLP mouse livers at various time points. Scale bar: 50 μm (upper), 10 μm (lower). (B) Quantification of LC3B intensity in the sham and CLP groups (n = 5/group). (C) Western blot analysis of BECLIN1, p62 and LC3B expression in liver tissues from sham and CLP mice. (D,E) Representative transmission electron microscopy (TEM) images (D) and autophagosome quantification (E) in sham and CLP mouse livers (n = 5 per group). Scale bar: 500 nm. Red arrows indicate autophagosomes. (B,E) Data are presented as the mean ± SD; *p < 0.05; **p < 0.01; ***p < 0.001; ns = not significant; one-way ANOVA.

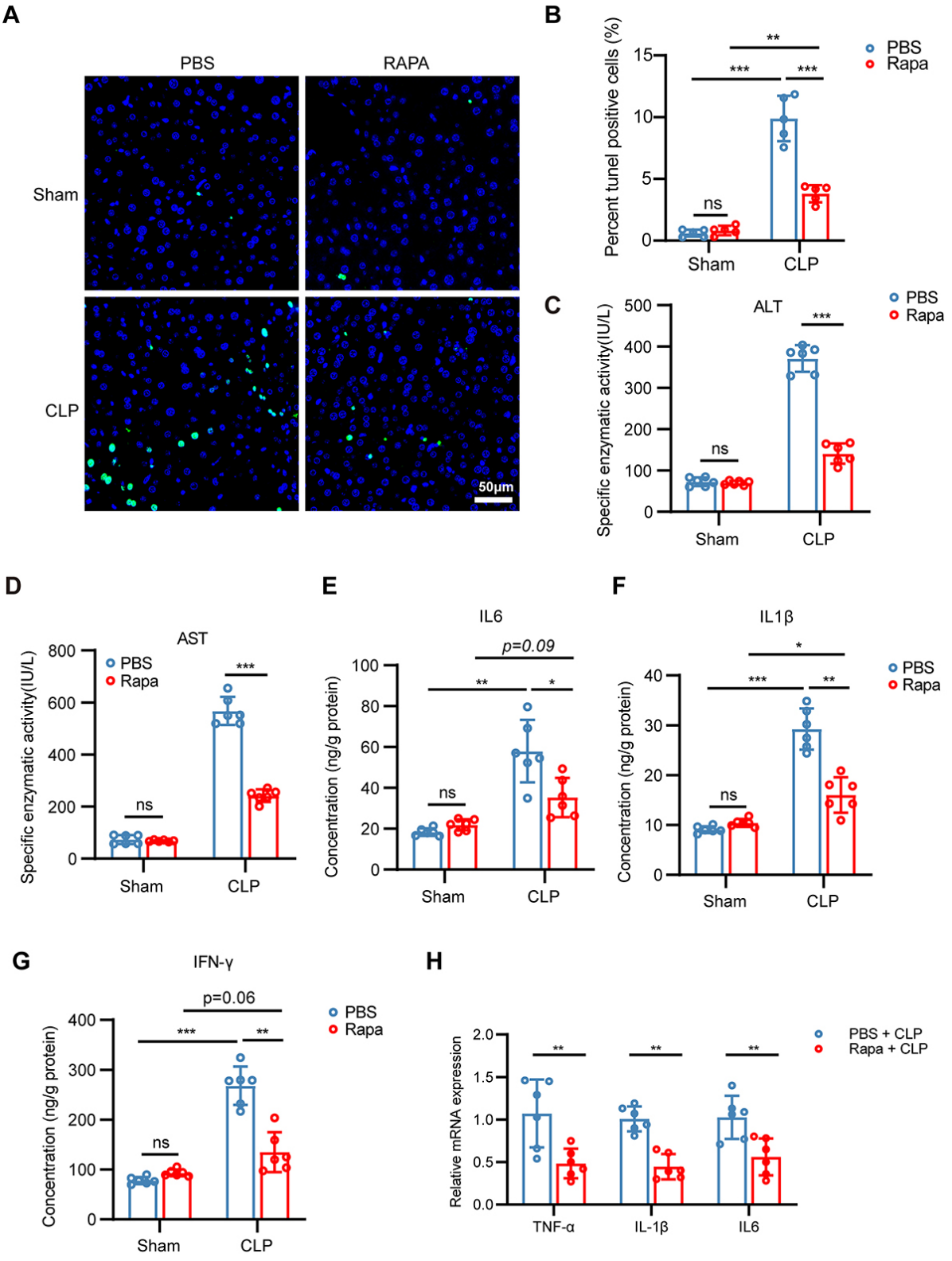

Fig. 4. Activation of autophagy protects against sepsis-induced liver injury. (A,B) Representative TUNEL staining (A) and quantification of TUNEL-positive cells (B) in sham and CLP mice pretreated with PBS or rapamycin (Rapa) for 36 hours. Scale bar: 50 μm. (C,D) Serum ALT (C) and AST (D) levels in sham and CLP mice pretreated with PBS or Rapa. (E–G) ELISA analysis of IL6, IL1β, and IFN-γ levels in serum from sham and CLP mice pretreated with PBS or Rapa. (H) qRT-PCR analysis of IL6, IL1β, and TNF-α mRNA expression in liver tissues from CLP mice pretreated with PBS or Rapa. (B–H) Data are presented as the mean ± SD; *$p < 0.05$; **$p < 0.01$; ***$p < 0.001$; ns = not significant; two-way ANOVA. n = 5 mice per group.

2.19 Statistical Analysis

Data are presented as the mean ± SD. Each mouse was considered an independent biological replicate. For cell experiments, biological replicates were defined as independent experiments performed on separately cultured cells. Technical replicates consisted of repeated measurements of the same biological sample and were performed in triplicate unless otherwise stated. Statistical analyses were performed using GraphPad Prism (version 8.0.2, San Diego, USA). Comparisons between two groups were made using a two-tailed unpaired Student's t-test. For multiple groups, one-way or two-way analysis of variance (ANOVA) was applied, followed by Tukey's or Bonferroni post hoc correction. High-throughput datasets (RNA-seq, microarray) were analyzed using the Wilcoxon test, with p values adjusted using the Benjamini–Hochberg method. Statistical significance was defined as $*p < 0.05$, $**p < 0.01$, and $***p < 0.001$; ns, not significant.

3. Results

3.1 Activation of Autophagy and the Inflammatory Response in Sepsis-induced Liver Injury

To investigate the role of autophagy in sepsis-induced liver injury (SILI), we reanalyzed RNA-seq data from mouse liver samples collected 24 hours after sepsis induction. Differential expression analysis revealed significant upregulation of inflammatory mediators, including Il6, Ccl20, and Cxcl1 (Fig. 1A,B). The upregulated genes were enriched in KEGG pathways related to apoptosis, mitophagy, and autophagy (Fig. 1C), while Gene Ontology analysis highlighted the regulation of the inflammatory response and autophagy (Fig. 1D). GSEA confirmed the significant enrichment of pathways related to autophagy and inflammation (Fig. 1E–I). These results suggest that SILI is characterized by the concurrent activation of autophagy and inflammatory pathways at 24 hours postsepsis.

3.2 Progressive Liver Injury and Inflammation in CLP-induced Sepsis

To validate the above findings, we established a cecal ligation and puncture (CLP) model of sepsis-induced liver injury and analyzed liver samples at different time points. H&E staining revealed progressive liver damage, with increased inflammatory cell infiltration, vacuolar degeneration, loss of sinusoidal architecture, and vascular congestion, which became more pronounced after 24 hours (Fig. 2A,C). TUNEL staining revealed a gradual increase in the number of apoptotic cells, with the greatest increase occurring at 36 hours (Fig. 2B,D). Serum ALT and AST levels progressively increased during the first 24 hours, followed by a sharp increase (Fig. 2E,F). qRT–PCR analysis of liver tissue revealed marked upregulation of the inflammatory cytokines IL6, TNFα, IL1β, and IFN-γ, particularly after 24 hours (Fig. 2G).

These results indicate that CLP-induced sepsis leads to progressive liver injury and inflammatory activation, with significant deterioration after 24 hours.

3.3 Temporal Dynamics of Autophagy in Sepsis-induced Liver Injury

To define autophagy dynamics during SILI, we assessed autophagic markers at different time points after CLP. Immunofluorescence staining for LC3B revealed a progressive increase in the number of LC3B puncta within the first 24 hours, indicating increased autophagic activity, followed by a marked decrease at 36 hours (Fig. 3A,B). Western blot analysis showed that BECLIN1 and LC3B levels increased during the first 24 hours and then decreased, whereas p62 decreased initially and subsequently increased (Fig. 3C). Electron microscopy confirmed a significant increase in autophagic structures at 24 hours post-CLP (Fig. 3D,E).

These results demonstrate that autophagy is transiently activated during the early phase of CLP-induced liver injury but decreases at later stages, which is correlated with the worsening of hepatic injury.

3.4 Activation of Autophagy Protects Against Sepsis-Induced Liver Injury

To evaluate the functional role of autophagy in SILI, mice were pretreated with rapamycin (Rapa) before CLP induction. Although Rapa did not affect the sham group, it markedly attenuated hepatocyte apoptosis in septic mice, as evidenced by fewer TUNEL-positive cells (Fig. 4A,B). Serum ALT and AST levels were markedly elevated after CLP but were significantly reduced by Rapa treatment (Fig. 4C,D). Similarly, Rapa pretreatment markedly attenuated the CLP-induced increases in serum IL6, IL1β, and IFN-γ levels (Fig. 4E–G) and hepatic IL6, IL1β, and TNF-α mRNA expression (Fig. 4H).

These results suggest that autophagy activation protects against SILI by limiting hepatocyte apoptosis, improving liver function, and suppressing hepatic inflammation.

3.5 Dynamic Changes and Role of Autophagy in SILI In Vitro

To simulate SILI *in vitro*, HepG2 cells were treated with LPS, and alterations in autophagy were assessed. Western blot and qRT–PCR analyses revealed increased LC3B-II and BECLIN1 levels at 12 hours, but these levels decreased at 24 hours (Fig. 5A–C). Cotreatment with chloroquine (CQ) increased LC3B-II accumulation at 12 hours, indicating increased autophagic flux. However, at 24 hours, autophagic activity was impaired, as evidenced by a reduction in LC3B fluorescence intensity (Fig. 5D,E). Next, apoptosis was assessed by PI staining (Fig. 5F,G) and qRT–PCR for Caspase3 and Bax (Fig. 5H,I), which revealed a time-dependent increase in apoptosis following LPS treatment, which was exacerbated by CQ.

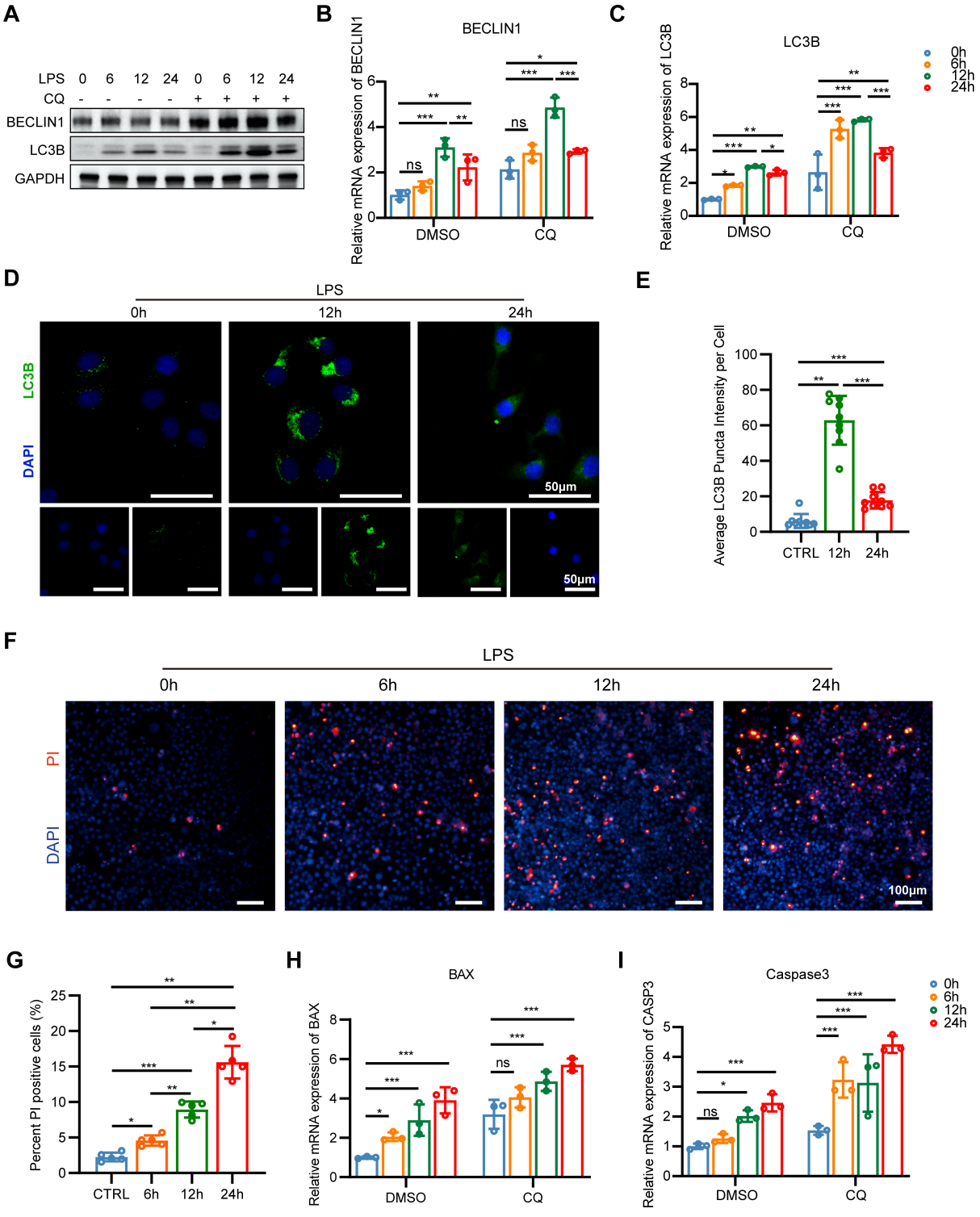

Fig. 5. Dynamic changes and role of autophagy in SILI *in vitro*. (A–C) Western blot (A) and qRT–PCR (B,C) analyses of LC3B-II and BECLIN1 in cells treated with LPS (400 ng/mL) with or without chloroquine (CQ, 10 μM) for the indicated time points (0, 6, 12, and 24 h). (D,E) Immunofluorescence staining of LC3B puncta (D) and quantification of mean fluorescence intensity per cell (E) in HepG2 cells treated with LPS for 0, 12, or 24 hours. All scale bars = 50 μm. (F,G) Representative propidium iodide (PI) staining images (F) and quantification of cell death (G) in LPS-treated HepG2 cells. All scale bars = 100 μm. (H,I) qRT–PCR analysis of Bax (H) and Caspase3 (I) mRNA expression levels in HepG2 cells treated with LPS with or without CQ. (B,C,E,G,H,I) Data are presented as the mean ± SD (n = 3–4/group; *$p < 0.05$; **$p < 0.01$; ***$p < 0.001$; ns = not significant; one-way ANOVA).

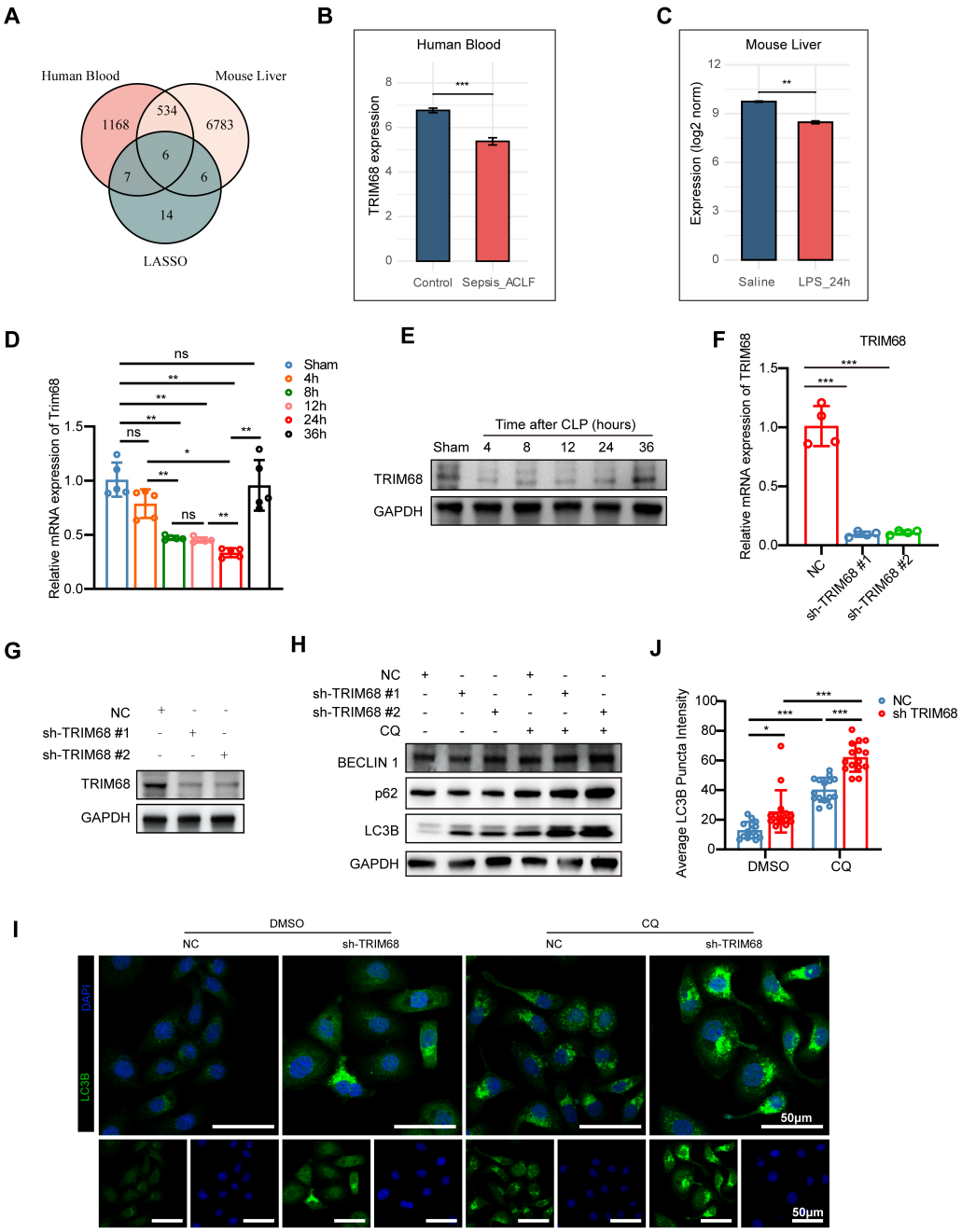

Fig. 6. Integrated human and mouse transcriptomics reveal TRIM68 as a negative regulator of autophagy in SILI. (A) Venn diagram showing the overlap among autophagy-related genes identified from human blood transcriptomic analysis, mouse liver differential expression analysis, and LASSO regression. (B,C) Expression levels of TRIM68 in human (B) and mouse liver (C) transcriptomic datasets. (D,E) qRT–PCR (D) and Western blot (E) analyses of TRIM68 expression in liver tissues from sham or CLP-induced SILI mice. $n = 5$ mice/group. (F,G) Validation of TRIM68 knockdown in HepG2 cells by qRT–PCR (F) and Western blotting (G). $n = 4$ per group. (H) Representative immunoblots of LC3B, BECLIN1, p62 and GAPDH (loading control) in knockdown negative control (NC) and TRIM68-knockdown HepG2 cells treated with LPS for 24 hours with or without the addition of CQ (10 μM). (I,J) Immunofluorescence staining of LC3B puncta (I) and quantification of fluorescence intensity (J) in NC and TRIM68-knockdown HepG2 cells treated with LPS for 24 hours and supplemented with DMSO or CQ (10 μM). All scale bars = 50 μm. $n = 15$ cells per group (three randomly selected cells per sample). (B–D,F,J) Data are presented as the mean ± SD; ns $p > 0.05$, *$p < 0.05$, **$p < 0.01$, ***$p < 0.001$ by Wilcoxon test (B,C), one-way ANOVA (D,F), or two-way ANOVA (J).

These results are consistent with the *in vivo* findings, which revealed transient autophagy activation early on, followed by impairment and worsened injury with autophagy inhibition.

3.6 Integrated Human and Mouse Transcriptomics Identify TRIM68 as a Negative Regulator of Autophagy in SILI

In sepsis-induced liver injury (SILI), liver tissue is often inaccessible, but previous studies have shown that blood transcriptomics can predict tissue-specific gene expression, with 60% of genes predicted on average, and up to 81% in skeletal muscle [15,16]. To investigate the molecular mechanisms of SILI, we integrated two publicly available human blood transcriptomic datasets from patients with sepsis (GSE142255 and GSE156382). Differential expression analysis revealed 2514 upregulated genes and 2841 downregulated genes (**Supplementary Fig. 1A,B**). Functional enrichment analyses revealed strong associations with pathways related to cellular senescence, immune activation, and inflammation (**Supplementary Fig. 1C–F**).

Intersection of DEGs with curated autophagy-related gene sets revealed 46 upregulated and 66 downregulated candidates (**Supplementary Fig. 2A–D**). LASSO regression refined this to 33 core genes (**Supplementary Fig. 2E**), with six genes, including TRIM68, consistently downregulated in both the human and mouse datasets (Fig. 6A–C). In CLP-induced mice, TRIM68 expression decreased early after CLP but increased later (Fig. 6D,E), suggesting its dynamic regulation during SILI. Interestingly, this dynamic change in TRIM68 expression is in contrast to the pattern observed for autophagy, which is initially activated and then decreased during the progression of SILI. We propose that TRIM68 expression changes drive the observed alterations in autophagic flux, with TRIM68 loss enhancing autophagy and providing protection against liver injury.

To assess this hypothesis, stable TRIM68-knockdown HepG2 cells were generated (Fig. 6F,G). TRIM68 knockdown increased LC3B-II accumulation in response to LPS and CQ, accompanied by decreased p62 levels, indicating increased autophagic flux (Fig. 6H). Immunofluorescence analysis further confirmed the increase in the number of LC3B puncta in the TRIM68-deficient cells (Fig. 6I,J).

Collectively, these results demonstrate that TRIM68 is dynamically regulated during SILI and functions as a negative regulator of autophagy, with its loss enhancing autophagic flux in SILI.

3.7 Loss of TRIM68 Enhances Autophagy by Stabilizing TIP60 and Promoting H4 Acetylation of Autophagy Genes

To investigate the mechanism by which TRIM68 inhibits autophagy, we first analyzed the transcriptional signatures associated with TRIM68 expression (**Supplementary Fig. 3A**). The functional enrichment of the TRIM68-correlated genes indicated their involvement in chromatin modification and chromatin organization (**Supplementary Fig. 3B**). Consistent with these findings, TRIM68 knockdown significantly increased the mRNA expression levels of genes associated with autophagy, including ATG13, ATG14, ATG2A, ULK1, SIRT1, BNIP3, CTNS, and CLN5, whereas TRIM68 overexpression suppressed the expression of these genes (Fig. 7A,B), suggesting that TRIM68 negatively regulates autophagy at the transcriptional level.

Given previous reports that TIP60 interacts with TRIM68 and that TIP60 is a key acetyltransferase for histone H4 acetylation, we next examined whether TRIM68 regulates autophagy through TIP60. Endogenous immunoprecipitation (IP) and coimmunoprecipitation (Co-IP) confirmed the stable interaction between TRIM68 and TIP60 (Fig. 7C,D). Immunofluorescence analysis further revealed clear colocalization of TRIM68 and TIP60 (Fig. 7E). Importantly, TRIM68 knockdown led to a marked increase in TIP60 protein levels, suggesting that TRIM68 normally restrains TIP60 abundance (Fig. 7F).

We further explored whether TRIM68 affects the acetylation of histone H4 at autophagy-related gene loci by influencing TIP60 expression. H4ac CUT&Tag revealed a significant increase in H4ac enrichment after TRIM68 knockdown (Fig. 7G), particularly at the promoter regions of key autophagy-related genes (Fig. 7H). Consistent with these findings, TIP60 overexpression rescued the TRIM68-mediated suppression of autophagy-related genes, further supporting that TIP60 acts downstream of TRIM68 to regulate autophagy. (Fig. 7I).

Collectively, these results demonstrate that the loss of TRIM68 enhances autophagy by stabilizing TIP60, leading to increased H4ac at autophagy gene promoters, which in turn activates the transcription of autophagy-related genes.

3.8 TRIM68 Loss Promotes Autophagy and Protects Against Liver Injury In Vivo

To further investigate the role of TRIM68 *in vivo*, wedelivered a TRIM68 knockdown plasmid via hydrodynamic tail vein injection and performed CLP 2 weeks postinjection, followed by analysis at 36 hours (Fig. 8A). TRIM68 loss significantly reduced the number of TUNEL-positive cells (Fig. 8B,C), indicating decreased apoptosis. Although the absolute reductions in ALT (from ~600 U/L to 400 U/L) and AST (from ~1600 U/L to 800 U/L) might seem modest, both were statistically significant and indicate meaningful improvements in liver function (Fig. 8D), and inflammatory cytokines were markedly reduced in both serum and liver tissue (Fig. 8E,F). These findings suggest that TRIM68 loss confers substantial functional improvements in liver injury.

Mechanistically, endogenous immunoprecipitation (IP) and immunofluorescence confirmed the colocalization of TRIM68 and TIP60 in liver tissue (Fig. 8G,H). TRIM68 loss promoted TIP60 expression and altered autophagy markers, increasing LC3B and decreasing p62 lev-

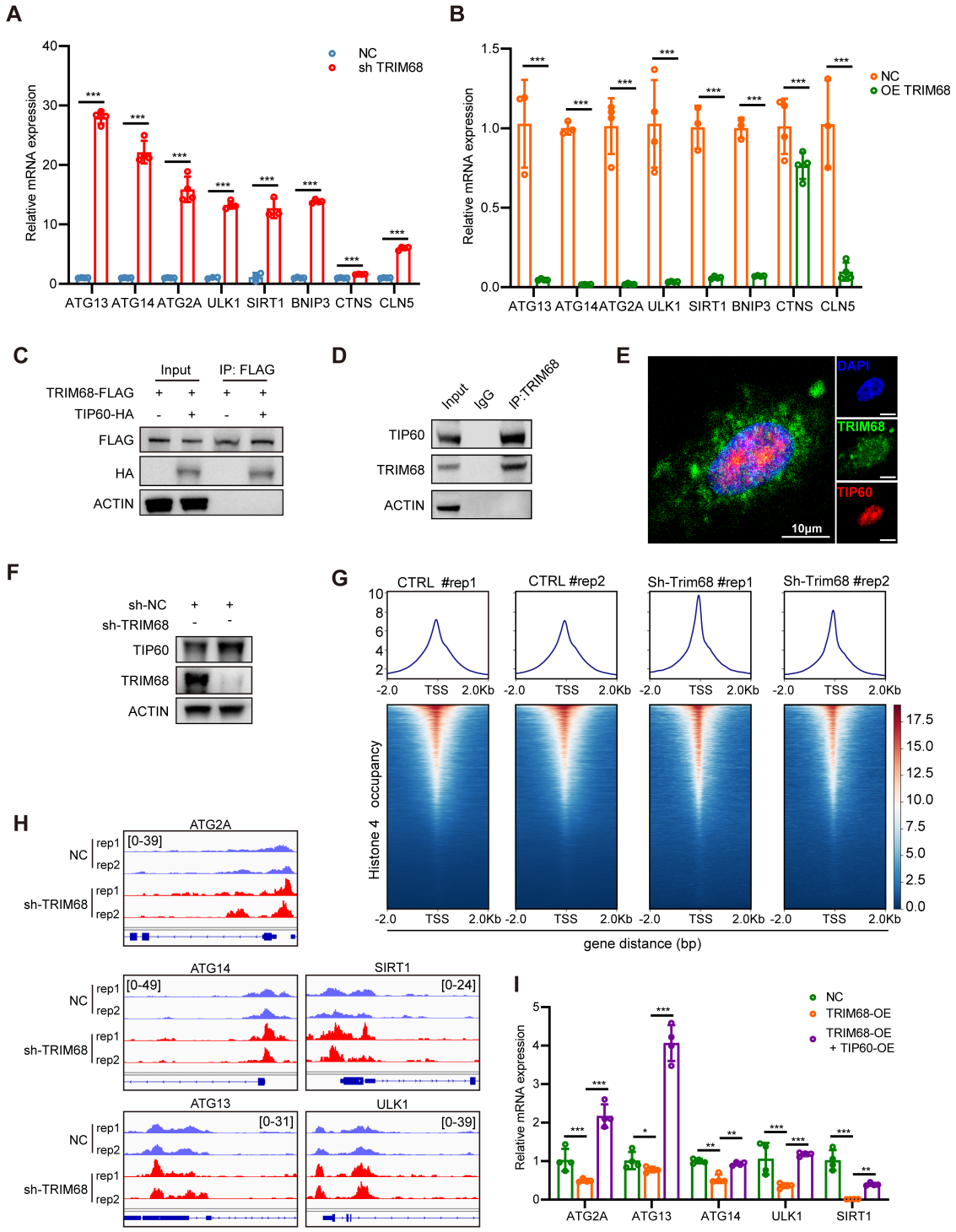

Fig. 7. Loss of TRIM68 enhances autophagy by stabilizing TIP60 and promoting H4 acetylation of autophagy genes. (A,B) mRNA levels of autophagy-related genes in TRIM68-knockdown (A) or TRIM68-overexpressing (OE) (B) HepG2 cells. (C,D) Co-IP (C) and endogenous IP (D) results showing the interaction between TRIM68 and TIP60 *in vitro*. (E) Representative immunofluorescence images costaining for TRIM68 (green), TIP60 (red), and DAPI (blue) in HepG2 cells. All scale bar = 10 μm. (F) Western blot analysis of TIP60 expression in NC- and TRIM68-shRNA-treated cells. (G,H) Cut-tag analysis of H4 acetylation (H4ac) across the genome (G) and at specific autophagy-related gene promoters (H) following TRIM68 knockdown. (I) qRT–PCR analysis of autophagy-related genes in the OE-NC, TRIM68-OE, and TRIM68-OE+ TIP60-OEgroups. (A,B,I) Data are presented as the mean ± SD; *$p < 0.05$; **$p < 0.01$; ***$p < 0.001$; one-way ANOVA.

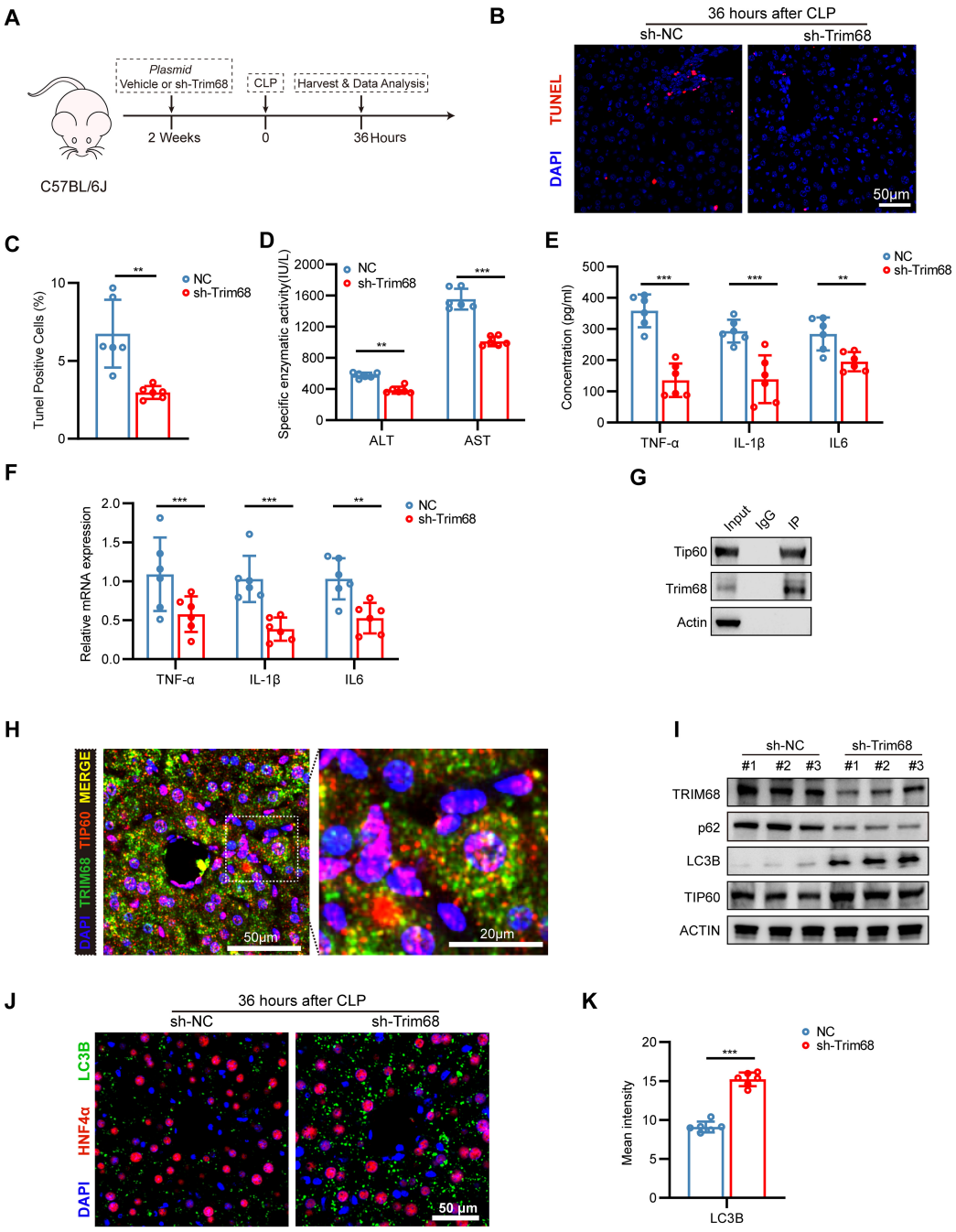

Fig. 8. TRIM68 loss promotes autophagy and protects against liver injury *in vivo*. (A) Experimental design for TRIM68 knockdown *in vivo*. n = 6/group. (B,C) Representative TUNEL staining (B) and quantification of apoptotic cells (C) in NC- and TRIM68-shRNA-treated mice after CLP. Scale bar = 50 μm. (D) Serum ALT and AST levels in the NC and TRIM68-shRNA-treated mice. (E,F) ELISA analysis of inflammatory cytokines in serum (E) and mRNA expression in liver tissue (F) from NC and TRIM68-shRNA mice after CLP. (G,H) Endogenous TRIM68 IP (G) and representative immunofluorescence images showing the colocalization of TRIM68 (green) and TIP60 (red) in the liver tissue of CLP mice (H). Scale bars = 50 μm (left panel) and 20 μm (magnified panel). (I) Western blot analysis of TRIM68, p62, LC3B, and TIP60 expression in sh-NC- or sh-TRIM68-treated mice after CLP. (J,K) Representative LC3B immunofluorescence images of liver tissues from shNC- and shTRIM68-treated mice post-CLP (J) and quantification of the average fluorescence intensity (K). Scale bar = 50 μm. (C–F,K) Data are presented as the mean ± SD; $^{**}p < 0.01$; $^{***}p < 0.001$; two-way ANOVA (C–F) or Student's *t* test.

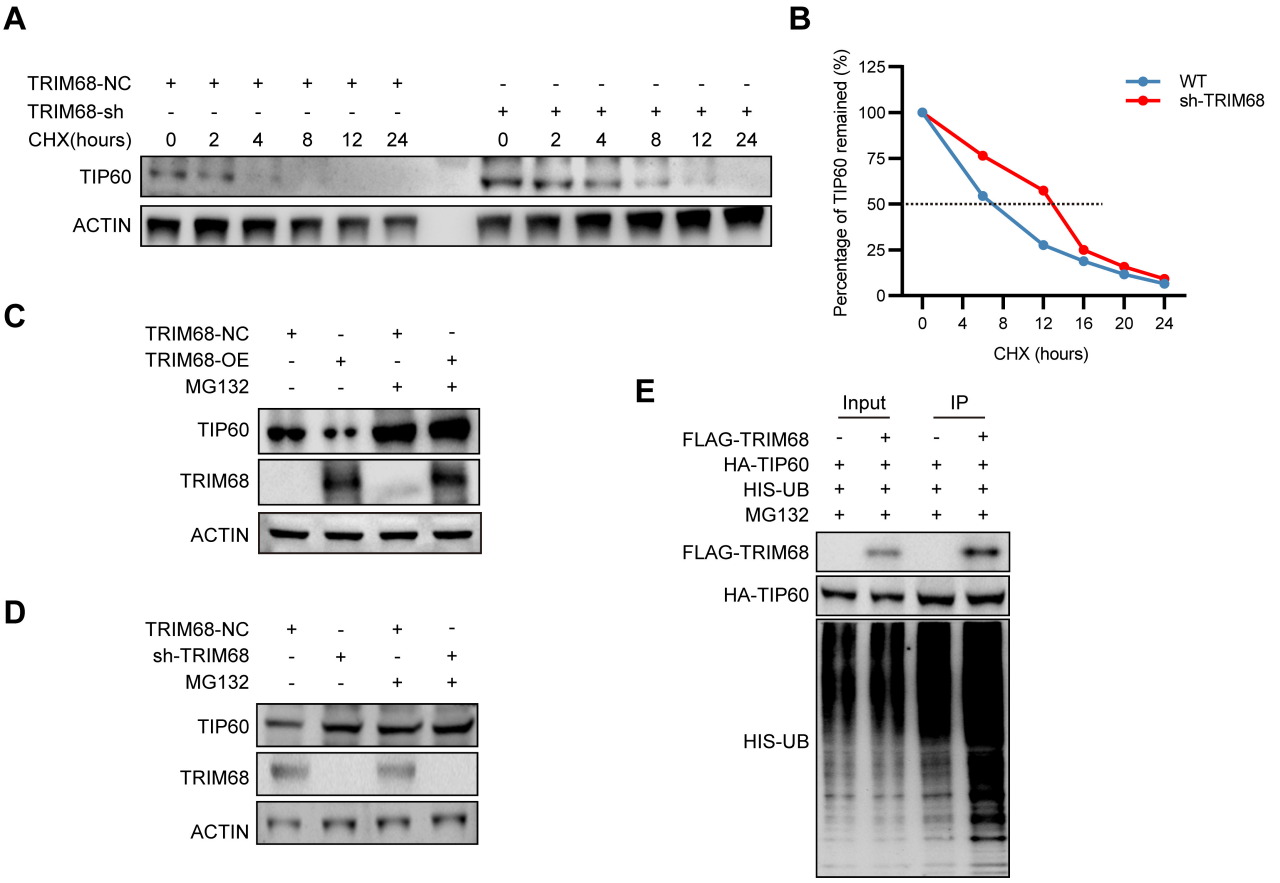

Fig. 9. TRIM68 Promotes TIP60 Ubiquitination and Degradation. (A,B) WT or shTRIM68-transfected HepG2 cells were treated with CHX (50 μg/mL) for the indicated times, and TIP60 stability was assessed by Western blotting, with ACTIN used as a control (A). Densitometry was used to estimate the half-life of TIP60 (B). (C,D) TRIM68-OE-NC and TRIM68-OE (C) or sh-TRIM68-NC and sh-TRIM68 (D) HepG2 cells were treated with MG132 (10 μM) for 10 hours, and the TRIM68 and TIP60 levels were measured by Western blotting. (E) HEK293T cells cotransfected with HA-TIP60, His-ubiquitin (UB), and FLAG or FLAG-TRIM68 were treated with 10 μM MG132 for 10 hours. Immunoprecipitation with anti-HA antibodies and Western blotting using HIS, HA, FLAG, and actin antibodies were used to analyze TIP60 ubiquitination.

els (Fig. 8I). Immunofluorescence further confirmed the significant increase in LC3B fluorescence intensity (Fig. 8J,K).

These results collectively suggest that TRIM68 loss enhances autophagic activity and provides protection against sepsis-induced liver injury through the promotion of TIP60-mediated autophagy.

3.9 TRIM68 Promotes TIP60 Ubiquitination and Degradation

To investigate how TRIM68 regulates TIP60 expression, we hypothesized that TRIM68 promotes TIP60 degradation via ubiquitination. Cycloheximide (CHX) chase assays revealed that TRIM68 knockdown significantly increased the half-life of TIP60 (Fig. 9A,B). MG132 treatment reversed the reduction in TIP60 expression induced by TRIM68 overexpression (Fig. 9C). Consistently, in shTRIM68-NC cells, the decrease in TIP60 expression was abolished following MG132 treatment, suggesting that TRIM68 promotes TIP60 degradation via the proteasomal pathway (Fig. 9D). Ubiquitination assays confirmed that TRIM68 overexpression enhanced TIP60 ubiquitination and degradation (Fig. 9E).

These results demonstrate that TRIM68 regulates TIP60 expression by promoting its ubiquitination and proteasomal degradation.

4. Discussion

Sepsis-induced acute liver injury (SILI), characterized by excessive inflammatory activation, is a critical determinant of poor outcomes in critically ill patients, highlighting the urgent need for effective therapeutic interventions [17]. Autophagy maintains hepatic homeostasis and restrains inflammation by clearing damaged organelles, limiting oxidative stress, and removing danger signals such as HMGB1, thereby suppressing NLRP3 inflammasome ac-

tivation and excessive cytokine release [7,18,19,20]. In SILI, autophagy is dynamically regulated, with early activation followed by a decrease that parallels the progression of liver injury. Consistent with previous studies showing autophagosome accumulation during early sepsis [11], our data suggest that this early activation is transient and insufficient to sustain effective autophagic flux, contributing to worsening liver damage. However, enhancing autophagy during its decline significantly alleviated hepatic injury and inflammatory responses, highlighting the protective role of autophagy in SILI.

Through integrated transcriptomic analyses of human and murine datasets, we identified TRIM68 as a negative regulator of autophagy in SILI, with TRIM68 loss enhancing autophagic flux, alleviating liver injury, and reducing inflammation. This protective effect is linked to the dynamic regulation of TRIM68, with expression decreasing early after sepsis induction and increasing at later stages, likely as a compensatory response. The observed changes in TRIM68 expression appear to drive alterations in autophagic flux, underscoring its role in modulating both autophagy and liver protection during SILI.

TRIM68, an E3 ubiquitin ligase within the tripartite motif-containing (TRIM) family, regulates protein turnover by promoting the ubiquitination and proteasomal degradation of TIP60 (KAT5), a key acetyltransferase involved in autophagy regulation [21]. Further investigation into TIP60, which regulates autophagy at both the post-translational and transcriptional levels, reveals that TIP60 activation occurs through acetylation at lysine residues K162 and K606, independent of mTORC1 and AMPK signaling [22,23]. TIP60 also promotes autophagic processes by modifying proteins such as SQSTM1 and Atg3 under stress conditions [22]. Notably, TIP60 enhances histone H4 acetylation at autophagy-related gene loci, driving the transcriptional activation of autophagy [24]. In line with these findings, our data demonstrate that the loss of TRIM68 stabilizes TIP60 by reducing its ubiquitination and proteasomal degradation, leading to increased histone H4 acetylation at autophagy-related genes and enhanced transcriptional activation. This mechanism ultimately promotes autophagic flux and attenuates inflammatory liver injury in SILI. Together, these findings establish a TRIM68–TIP60–H4ac regulatory axis that links ubiquitin-mediated protein turnover to the epigenetic control of autophagy.

Nevertheless, this study has several limitations. While protective effects were observed, our analysis covers only a short window of disease progression, and further studies with multiple time points are needed to understand the long-term impact of TRIM68 loss. Validation in human cell models and peripheral blood provides valuable insights, but due to limited clinical liver samples, further validation in human liver tissue is needed. Additionally, the upstream regulators of TRIM68 and specific ubiquitination sites of TIP60 require further investigation. Future research on these issues will be crucial to fully define the translational potential of the TRIM68–TIP60 axis in sepsis-induced liver injury.

5. Conclusion

Our study identified TRIM68 as a potential therapeutic target for modulating autophagy in SILI. Targeting TRIM68 to relieve the suppression of TIP60 activity may restore autophagic activity and mitigate liver injury during sepsis, thus providing a mechanistic framework for therapeutic targeting.

Availability of Data and Materials

The public transcriptomic datasets analyzed during the current study are available in the Gene Expression Omnibus (GEO) repository, https://www.ncbi.nlm.nih.gov/geo/, under accession numbers GSE167277, GSE142255, and GSE156382. The CUT&Tag dataset generated in this study has been deposited in GEO under accession number GSE326879. Other data supporting the findings of this study are available from the corresponding author upon reasonable request.

Author Contributions

MS and HY conceived and supervised the study, and secured funding. YX designed and performed the experiments, and wrote the original manuscript. XY constructed the animal models and collected samples. XC guided the bioinformatics analysis and optimized the figures. All authors contributed to editorial changes in the manuscript. All authors read and approved the final manuscript. All authors have participated sufficiently in the work and agreed to be accountable for all aspects of the work.

Ethics Approval and Consent to Participate

All animal experiments were approved by the Animal Ethics Committee of Anhui Medical University (Approval No. LLSC20242499) and conducted in accordance with the National Institutes of Health Guide for the Care and Use of Laboratory Animals.. The study was carried out in accordance with the ARRIVE guidelines. No human participants were involved in this study.

Acknowledgment

We gratefully acknowledge the technical support provided by the Animal Experiment Center of Anhui Medical University. We also thank the GEO database for providing publicly available transcriptomic datasets used in this study.

Funding

This work was supported by grants from the National Natural Science Foundation of China (No. 82370605) and the Hefei Municipal Health Commission Science and Technology Project (No. Hwk2025yb001).

Conflicts of Interest

The authors declare that they have no competing interests.

Declaration of AI and AI-Assisted Technologies in the Writing Process

During the preparation of this work, the authors used ChatGPT-5 and DeepSeek-V3 to check spelling, grammar, and general language clarity. After using these tools, the authors reviewed, edited, and took full responsibility for the entire content of this publication.

Supplementary Material

Supplementary material associated with this article can be found, in the online version, at https://doi.org/10.31083/FBL50519.

References

[1] Singer M, Deutschman CS, Seymour CW, Shankar-Hari M, Annane D, Bauer M, et al. The Third International Consensus Definitions for Sepsis and Septic Shock (Sepsis-3). JAMA. 2016; 315: 801–810. https://doi.org/10.1001/jama.2016.0287

[2] Vincent JL, Ince C, Pickkers P. Endothelial dysfunction: a therapeutic target in bacterial sepsis? Expert Opinion on Therapeutic Targets. 2021; 25: 733–748. https://doi.org/10.1080/14728222.2021.1988928

[3] Reinhart K, Daniels R, Kissoon N, Machado FR, Schachter RD, Finfer S. Recognizing Sepsis as a Global Health Priority - A WHO Resolution. The New England Journal of Medicine. 2017; 377: 414–417. https://doi.org/10.1056/NEJMp1707170

[4] Strnad P, Tacke F, Koch A, Trautwein C. Liver - guardian, modifier and target of sepsis. Nature Reviews. Gastroenterology & Hepatology. 2017; 14: 55–66. https://doi.org/10.1038/nrgastro.2016.168

[5] Yan J, Li S, Li S. The role of the liver in sepsis. International Reviews of Immunology. 2014; 33: 498–510. https://doi.org/10.3109/08830185.2014.889129

[6] Choi AMK, Ryter SW, Levine B. Autophagy in human health and disease. The New England Journal of Medicine. 2013; 368: 651–662. https://doi.org/10.1056/NEJMra1205406

[7] Li Y, Xu J, Chen W, Wang X, Zhao Z, Li Y, et al. Hepatocyte CD36 modulates UBQLN1-mediated proteasomal degradation of autophagic SNARE proteins contributing to septic liver injury. Autophagy. 2023; 19: 2504–2519. https://doi.org/10.1080/15548627.2023.2196876

[8] Lin CW, Lo S, Perng DS, Wu DBC, Lee PH, Chang YF, et al. Complete activation of autophagic process attenuates liver injury and improves survival in septic mice. Shock (Augusta, Ga.). 2014; 41: 241–249. https://doi.org/10.1097/SHK.0000000000000111

[9] Oami T, Watanabe E, Hatano M, Teratake Y, Fujimura L, Sakamoto A, et al. Blocking Liver Autophagy Accelerates Apoptosis and Mitochondrial Injury in Hepatocytes and Reduces Time to Mortality in a Murine Sepsis Model. Shock (Augusta, Ga.). 2018; 50: 427–434. https://doi.org/10.1097/SHK.0000000000001040

[10] Lalazar G, Ilyas G, Malik SA, Liu K, Zhao E, Amir M, et al. Autophagy confers resistance to lipopolysaccharide-induced mouse hepatocyte injury. American Journal of Physiology. Gastrointestinal and Liver Physiology. 2016; 311: G377–G386. https://doi.org/10.1152/ajpgi.00124.2016

[11] Watanabe E, Muenzer JT, Hawkins WG, Davis CG, Dixon DJ, McDunn JE, et al. Sepsis induces extensive autophagic vacuolization in hepatocytes: a clinical and laboratory-based study. Laboratory Investigation; a Journal of Technical Methods and Pathology. 2009; 89: 549–561. https://doi.org/10.1038/labinvest.2009.8

[12] Yu Q, Zou L, Yuan X, Fang F, Xu F. Dexmedetomidine Protects Against Septic Liver Injury by Enhancing Autophagy Through Activation of the AMPK/SIRT1 Signaling Pathway. Frontiers in Pharmacology. 2021; 12: 658677. https://doi.org/10.3389/fphar.2021.658677

[13] Cho HI, Kim SJ, Choi JW, Lee SM. Genipin alleviates sepsis-induced liver injury by restoring autophagy. British Journal of Pharmacology. 2016; 173: 980–991. https://doi.org/10.1111/bph.13397

[14] Rittirsch D, Huber-Lang MS, Flierl MA, Ward PA. Immunodesign of experimental sepsis by cecal ligation and puncture. Nature Protocols. 2009; 4: 31–36. https://doi.org/10.1038/nprot.2008.214

[15] Basu M, Wang K, Ruppin E, Hannenhalli S. Predicting tissue-specific gene expression from whole blood transcriptome. Science Advances. 2021; 7: eabd6991. https://doi.org/10.1126/sciadv.abd6991

[16] Xu W, Liu X, Leng F, Li W. Blood-based multi-tissue gene expression inference with Bayesian ridge regression. Bioinformatics (Oxford, England). 2020; 36: 3788–3794. https://doi.org/10.1093/bioinformatics/btaa239

[17] Ho J, Yu J, Wong SH, Zhang L, Liu X, Wong WT, et al. Autophagy in sepsis: Degradation into exhaustion? Autophagy. 2016; 12: 1073–1082. https://doi.org/10.1080/15548627.2016.1179410

[18] Aki T, Unuma K, Uemura K. Emerging roles of mitochondria and autophagy in liver injury during sepsis. Cell Stress. 2017; 1: 79–89. https://doi.org/10.15698/cst2017.11.110

[19] Nakahira K, Haspel JA, Rathinam VAK, Lee SJ, Dolinay T, Lam HC, et al. Autophagy proteins regulate innate immune responses by inhibiting the release of mitochondrial DNA mediated by the NALP3 inflammasome. Nature Immunology. 2011; 12: 222–230. https://doi.org/10.1038/ni.1980

[20] Zhang YY, Ning BT. Signaling pathways and intervention therapies in sepsis. Signal Transduction and Targeted Therapy. 2021; 6: 407. https://doi.org/10.1038/s41392-021-00816-9

[21] Huang N, Sun X, Li P, Liu X, Zhang X, Chen Q, et al. TRIM family contribute to tumorigenesis, cancer development, and drug resistance. Experimental Hematology & Oncology. 2022; 11: 75. https://doi.org/10.1186/s40164-022-00322-w

[22] Xu Y, Wan W. Acetylation in the regulation of autophagy. Autophagy. 2023; 19: 379–387. https://doi.org/10.1080/15548627.2022.2062112

[23] Lin SY, Li TY, Liu Q, Zhang C, Li X, Chen Y, et al. GSK3-TIP60-ULK1 signaling pathway links growth factor deprivation to autophagy. Science (New York, N.Y.). 2012; 336: 477–481. https://doi.org/10.1126/science.1217032

[24] Yu YS, Shin HR, Kim D, Baek SA, Choi SA, Ahn H, et al. Pontin arginine methylation by CARM1 is crucial for epigenetic regulation of autophagy. Nature Communications. 2020; 11: 6297. https://doi.org/10.1038/s41467-020-20080-9